Broad Substrate Specificity and Catalytic Mechanism of *Pseudomonas stutzeri* L-Rhamnose Isomerase: Insights from QM/MM Molecular Dynamics Simulations†

Ruibo Wu,‡ Hujun Xie,‡ Yirong Mo,‡,§ and Zexing Cao*,‡

Department of Chemistry and State Key Laboratory of Physical Chemistry of Solid Surfaces, College of Chemistry and Chemical Engineering, Xiamen University, Xiamen 361005, China, and Department of Chemistry, Western Michigan University, Kalamazoo, Michigan 49008

Received: February 5, 2009; Revised Manuscript Received: April 16, 2009

L-Rhamnose isomerase (L-RhI) has been found in many microorganisms and catalyzes the reversible isomerization between L-rhamnose and L-rhamnulose. Interestingly, *Pseudomonas stutzeri* L-RhI (*P. stutzeri* L-RhI) exhibits a much broader substrate specificity than others such as *Escherichia coli* L-RhI (*E. coli* L-RhI) and catalyzes the interconversion of many aldoses and ketoses. To elucidate the uniqueness of *P. stutzeri* L-RhI and the mechanism of enzymatic catalysis, we performed dual-level combined QM/MM molecular dynamics simulations on *P. stutzeri* L-RhI with a number of substrates. Calculations show that the reversible process between aldoses and ketoses can be rationalized by a zwitterion intermediate mechanism that involves both proton and hydride transfers. Predicted free energy barriers in the rate-determining step are 8.9 kcal/mol for L-rhamnose and 13.6 kcal/mol for D-allose, respectively, in good agreement with the experimental characterization of relative substrate reactivity. Conformational and hydrogen bond analyses of the active domain and evaluation of electrostatic and van der Waals (vdW) interactions between substrates and surrounding residues provide a basis to understand the catalytic role of conserved residues, the substrate specificity, and the relative activity of favorable substrates in *P. stutzeri* L-RhI.

Introduction

Enzymatic reactions can be executed efficiently under mild conditions and are essentially involved in all life processes. Their fascinating advantages over traditional chemical methods have inspired widespread industrial interests in enzymatic procedures that have been applied to the synthesis of rare carbohydrates and reactions concerning heat-sensitive substrates.[1−5] The well-characterized phosphoglucose isomerases (PGI) and bifunctional phosphoglucose/phosphhomannose isomerases (PGI/PMI) form a PGI superfamily that catalyze the isomerization of phosphorylated carbohydrates,[6−9] whereas several well-known D-xylose isomerase (D-XI), L-fucose isomerase, L-arabinose isomerase, and L-rhamnose isomerase work on unphosphorylated substrates. Except for the cupin-type PGIs, the function of conventional PGIs does not require metal ions in the active domain. In contrast, metal ions are prerequisite for enzymes catalyzing the reversible isomerization of unphosphorylated sugars.[10−13] For example, the isomerization activity of D-XI from *S. rubiginosus* completely depends on a divalent ion such as Mg^{2+}, Co^{2+}, or Mn^{2+}, and D-XI has been widely used in the commercial production of high-fructose corn syrup.[14,15]

L-Rhamnose isomerase (L-RhI), which is responsible for the reversible aldose-ketose interconversion of L-Rhamnose to L-Rhamnulose, has been found to play an important role in the rhamnose metabolism in *Escherichia coli*,[13,16] *Salmonella*,[17] *Lactobacillus*,[18] and *Pseudomonas*.[19] Its industrial applications in the rare sugar production have also been extensively exploited.[20−24] L-RhI from *Pseudomonas stutzeri* (*P. stutzeri* L-RhI), expressed in *Escherichia coli* as a recombinant His-tagged *P. stutzeri* L-RhI,[25,26] showed a broader substrate specificity than L-RhI from *Escherichia coli* (*E. coli* L-RhI). *P. stutzeri* L-RhI can efficiently catalyze the isomerization between L-rhamnose and L-rhamnulose, L-mannose and L-fructose, L-lyxose and L-xylulose, D-ribose and D-ribulose, and D-allose and D-psicose. The aldose structures of selected five-favored substrates are illustrated in Scheme 1, where L-mannose, L-xylose, and D-allose are normally considered as "rare sugars" due to their scarcity in nature. These rare sugars have become increasingly significant in food manufacture and health care, and many efforts aimed at facilitating the mass production of various rare and commercially expensive sugars have been made.[26]

Clearly, static X-ray crystallographic structures can provide indispensable structural information to understand the difference from *P. stutzeri* L-RhI to other L-RhIs such as *E. coli* L-RhI, and fortunately, both crystal structures of *E. coli* L-RhI and *P. stutzeri* L-RhI have been determined.[27] The sequence alignment of these two enzymes shows that their sequence identity is merely 17%,[25,26] suggesting that *P. stutzeri* L-RhI may quite differ from *E. coli* L-RhI structurally. But the crystal structures revealed that the amino acid residues bound to the metal site are well conserved in these two enzymes. Furthermore, structures of *P. stutzeri* L-RhI in complex with the substrate L-rhamnose or D-allose indicate that both substrates are nicely located in the substrate-binding site. Significantly, one part of the substrate-binding site in *P. stutzeri* L-RhI interacting with the substrate at positions 1, 2, and 3 (see Scheme 1) is identical with that in *E. coli* L-RhI, while the rest interacting with the fourth, fifth, and sixth positions is similar to the case of D-XI. On the basis of the comparison of these three-dimensional structures, it has been assumed that the configurations of the C2 and C3 positions of the substrate are closely associated with

† Part of the "Walter Thiel Festschrift".

* To whom correspondence should be addressed. E-mail: zxcao@xmu.edu.cn.

‡ Xiamen University.

§ Western Michigan University.

10.1021/jp901093g CCC: $40.75
Published on Web 05/27/2009

SCHEME 1: Fischer Projection Structures of Substrates Catalyzed by *P.stutzeri* L-RhI

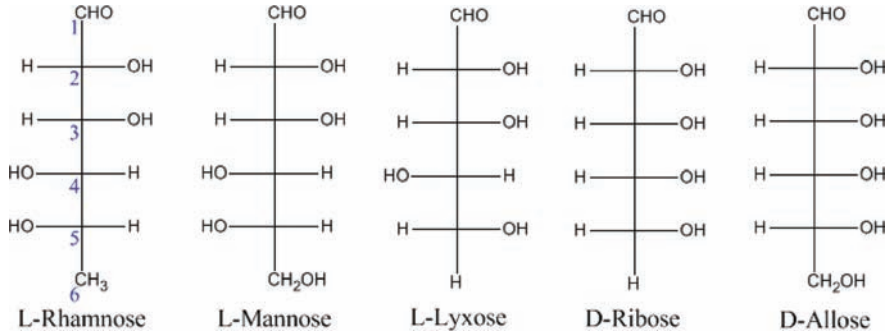

the enzyme activity,[28] while the configurations of C4 and C5 of the substrate do not remarkably affect the enzyme activity. In *E. coli* L-RhI, the presence of a hydrophobic pocket at the fourth, fifth, and sixth positions results in the strict substrate recognition. In sharp contrast, there is no such local hydrophobic environment around the substrate in *P. stutzeri* L-RhI, and this disparity may well explain the broad substrate specificity of *P. stutzeri* L-RhI in comparison with *E. coli* L-RhI.

Unfortunately, the current X-ray diffraction data are unable to completely identify the metal ions in *P. stutzeri* L-RhI, and the most probable candidates are Zn^{2+} or Mn^{2+} or Ni^{2+}. The electron density profiles of two metal ions (M-1 and M-2) show the M-1 is bound more tightly than the M-2 in the active site. The M-1 is generally considered to play a structural role in the substrate binding, while the role of M-2 is primarily catalytic as M-2 mediates the hydride shift between C1 and C2.[28,29] The metal-mediated hydride shift mechanism has also been proposed for the enzymatic reaction in D-XI.[30]

Despite static X-ray crystallographic studies on L-RhIs from various bacteria strains provide strong clues to elucidate the substrate recognition features and the enzyme activity, detailed mechanisms for the broad substrate specificity of *P. stutzeri* L-RhI and the enzymatic catalysis are elusive due to the lack of experimental evidence for the enzymatic dynamics and reaction transition states. In the present work, we intend to perform computational studies that can provide complementary information on bindings and reactions at the atomic and electronic level. To this end, molecular dynamics (MD) simulations on the aldose−ketose isomerization reaction catalyzed by *P. stutzeri* L-RhI have been performed at the combined QM/MM level. Possible reaction mechanisms for the reversible isomerization and roles of the conserved residues and the interface residues from the neighboring monomer have been investigated and elucidated.

Computational Methods

Combined QM/MM methods have been widely used for computational studies of biological systems.[31−41] Within the QM/MM model, the substrate and its surrounding key residues, which are directly involved in bond breakings and formations, are usually defined as the QM part and thus treated quantum-mechanically, whereas the rest of the protein and solvent is represented by force fields. This strategy combines the applicability and accuracy of QM methods in the description of chemical bond changes and the computational efficiency of MM approaches for large molecular systems. In consideration of the complex electronic structures of the transition-metal center and its ligand environment in metalloenzymes, the treatment of the QM part normally requires the DFT methodology, which may well balance the computational cost and the accuracy. As a matter of fact, the use of DFT approaches in QM/MM calculations has become increasingly popular.[42−44]

In computational studies aiming at correlating the structures, dynamics, and functions of proteins, it is essential to conduct MD simulations on the biological processes, where the QM part is often treated at the semiempirical theoretical level, such as AM1,[45] PM3,[46] and SCCDFTB,[47] to reduce the computational cost and guarantee enough samplings for the evaluation of thermodynamic and dynamic properties. But it is well-known that semiempirical methods may generate poor results and continuing efforts have been made to improve the reliability of these methods by either reoptimizing the parameters[48] or including d orbitals.[49−52] In this work, however, we employed a dual-level QM/MM approach[53,54] to generate potential of mean force (PMF) profiles. In dual-level (DL) MD simulations, the energy profile from PM3/MM MD simulations is named as the "low-level (LL)" PMF, while the "high-level(HL)" energy calculation is performed at the B3LYP/6-31G** level. In the PM3 calculations, the newly developed ZnB (zinc, biological) parameters,[55] which upgrade the description of zinc-containing metalloenzymes as compared with the original PM3 parameters for zinc,[56] was adopted. The dual-level total energy (E) and the dual-level PMF (W) can be expressed as follows:

$$E_{\mathrm{tot}}^{\mathrm{DL}} = E_{\mathrm{QM}}^{\mathrm{HL}} + \Delta E_{\mathrm{QM/MM}}^{\mathrm{LL}} + E_{\mathrm{MM}} \quad (1)$$

$$W^{\mathrm{DL}}(\xi) = W^{\mathrm{LL}}(\xi) + [E_{\mathrm{QM}}^{\mathrm{HL}}(\xi_{\mathrm{LL}}^{\mathrm{MEP}}) - E_{\mathrm{QM}}^{\mathrm{LL}}(\xi_{\mathrm{LL}}^{\mathrm{MEP}})] + \Delta W_0 \quad (2)$$

where ξ is the reaction coordinate, $\xi_{\mathrm{LL}}^{\mathrm{MEP}}$ indicates that the correction term was obtained along the minimum energy reaction path (MEP) at the low level of theory, and ΔW_0 is the energy difference between the high level and the low level at the reaction state. As shown in eq 2, the dual-level PMF may be improved by combining the sampling efficiency of PM3/MM MD simulations and the energy veracity of the QM subsystem at the high level of theory, and this strategy is very similar to the ONIOM model.[57] The dual-level approach has been used in previous QM/MM simulations.[53,54,58,59] Computational details for the correction term were presented in Figure 3S in the Supporting Information, and corresponding energy calculations were carried out with the Gaussian03 package.[60]

All computational models in this work were generated on the basis of the crystal structures of *P. stutzeri* L-RhI in complex with the bound substrates L-rhamnose and D-allose (PDB codes: 2I56 and 2I57). Since both X-ray structures are quite similar and the contact areas between chain A and chain B is significant for the enzymatic catalysis,[28] both the chains A and B from

PDB 2I56 were considered in the setup of computational models. The substitution of various substrates (see Scheme 1) for L-rhamnose generated initial models for these enzyme−substrate complexes. Hydrogen atoms of the protein were added by using the HBUILD facility in CHARMM[61] based on heavy atom positions and standard bond lengths and angles. The protonation states of histidine residues were determined on the basis of their individual microenvironments. Afterward, these enzyme−substrate models were solvated into a water sphere of 30 Å radius centered on the middle point of two zinc ions to produce initial computational models in solution. The final models of these complexes consist of about 19 950 atoms (see Figure 1a), including the protein, 858 crystal water molecules, ∼1500 water molecules from the water sphere, the substrate, and 8 sodium ions to neutralize the whole system.

During the MD simulations, about 90 atoms were included in the QM part, which consists of Glu219, Lys221, Asp254, His257, His281, His289, Asp327, two zinc cations, the substrate (L-rhamnose/L-mannose/L-lyxose/D-ribose/D-allose), and two crystal water molecules (CW625 and CW777). The QM/MM boundary was described with the generalized hybrid orbital (GHO) method.[62] A set of hybrid orbitals for each boundary atom between the QM and MM fragments were dynamically determined and one of the hybrid orbitals was involved in the SCF calculation for the QM region. The QM/MM boundaries are shown in Figure 1e. CHARMM22 and CHARMM27 force fields[63,64] were used to represent all of the MM atoms, and all chemical bonds with hydrogen atoms in the MM part were constrained with the SHAKE algorithm.[65] Stochastic boundary MD simulations at 300 K were carried out with CHARMM.[61] In the simulations, the reaction zone was defined as a sphere of 25 Å radius, and atoms in the reaction zone were propagated according to the Newtonian mechanics. Atoms within 25−30 Å comprised the buffer zone and were retained by a harmonic restraining force and propagated by Langevin dynamics. The harmonic force constants in units of kcal·mol^{-1}·A^{-2} were 1.22 for backbone oxygen atoms, 1.30 for other backbone atoms, and 0.73 for all side-chain atoms. The friction coefficients for heavy atoms of protein and the oxygen atoms of water molecules were assigned as 200 and 62 ps^{-1}, respectively. All atoms beyond 30 Å from the center were defined as the reservoir zone, which were fixed during the MD simulations. The effect imposed by the atoms in the reservoir zone was simulated by stochastic boundary potentials.[61,66] For the water molecules, the TIP3P potential[67] was used. The list of nonbonded interactions was truncated at 14 Å and the van der Waals and electrostatic interactions were smoothly switched off in the range 12−13 Å. The structural comparison and rmsd profiles between the crystal structure and the equilibrated structure from 300 ps MD simulations were shown in Figure 1S in Supporting Information.

The umbrella sampling technique was adopted to generate the low-level PMF along a designated reaction coordinate in the equilibrated model. A biasing harmonic potential with a force constant of 15−30 kcal/mol was imposed in MD simulations for all windows separated by 0.2 Å along the reaction coordinate. We note that the sufficient sampling for each window was essential for the reliable estimation of reaction barriers and the determination of intermediate states. The detailed comparison of PMFs starting from different initial configurations and different sampling time scales was outlined in Figure 2S in Supporting Information. The test MD simulations suggested that at least 100 ps MD simulations should be performed to reach the equilibrium state for each window.

To evaluate the equilibrated configurations of *P. stutzeri* L-RhI with various substrates from 300 ps PM3/MM MD simulations and relative energy profiles for isomerizations of the substrates, we also performed the QM/MM geometry optimizations at the DFT/CHARMM level. In the QM(DFT)/MM optimizations, the QM region remained the same as that in QM(PM3)/MM MD simulations, and the QM part and 2706 MM atoms (defined by including all residues around two zincs within a distance of 15 Å) were allowed to relax, whereas the remaining MM atoms were frozen. The QM part was treated at the B3LYP/6-31G(d) level and the MM part was described by the CHARMM force fields. An electronic embedding scheme[68] incorporating the MM charges into the one-electron Hamiltonian of the QM treatment and hydrogen link atoms with charge shift model[69,70] for the QM/MM boundary were adopted in the QM/MM treatment. The ChemShell package[71] integrating the Turbomole[72] and DL-POLY[73] programs were employed to perform the QM/MM computations. The default convergence criteria were adopted in the QM/MM geometry optimization with the HDLC optimizer[74] for complexes of the enzyme with the substrate L-rhamnose. For comparison with the dual level DFT:PM3/MM PMF, a potential energy surface scan at the QM(DFT)/MM level was also carried out.

Results and Discussion

I. Structures of the Active Site. The skeletal configurations of enzyme−substrate complexes in solution reached equilibrium and fluctuated only slightly after 100 ps in MD simulations, and the overall deviation of the 300 ps MD conformation of protein with reference to the crystal structure[28] was small (see Figure 1S in Supporting Information). Figure 1 displays the equilibrium conformation and structures of selected parts of the active domain. The zinc ions are located at the center of the large domain with a $(\beta/\alpha)_8$ barrel fold. Important residues forming the substrate-binding site in the equilibrated state of the enzyme with L-rhamnose are shown in Figure 1b, where the interactions of the substrate with its surrounding residues at the first, second, and third positions of the substrate are equivalent to those in *E. coli* L-RhI, while the interactions at the fourth, fifth, and sixth positions are similar to those in D-XI. Such structural characteristics in the active domain are the same as shown in the reported crystal structures.[28] The experimentally proposed conserved residues, two crystal water molecules, and other key residues in the substrate-binding site are survived during MD simulations. On the other hand, several water molecules gradually enter into the active site around the 4, 5, and 6 positions of the substrate (see Figure 1b). As Figure 1 shows, there is a large cavity in the substrate-binding site that can accommodate various substrates such as plotted in Scheme 1. These substrates differ from one another due to the *R*/*S* enantiotropy at the fourth and fifth positions and the group at the sixth position.

The coordination shell of Zn1 ("structural") changes little after 300 ps MD simulations, while the coordination shell of Zn2 ("catalytic") fluctuates slightly. As shown in Figure 1c, in the complex with L-rhamnose, Zn1 is ligated with the O2 and O3 atoms of L-rhamnose, the OD1 atom of Asp254, the ND1 atom of His281, the OE2 atom of Glu219, and the OD2 atom of Asp327. Similarly, the Zn2 ion is also hexacoordinated with ligands L-rhamnose, Asp289, His257, and two water molecules. In consideration of the slight change of the Zn2 coordination shell, we also carried out combined DFT/MM optimizations, and a comparison of the selected calculated and experimental bond lengths are collected in Table 1S in Supporting Informa-

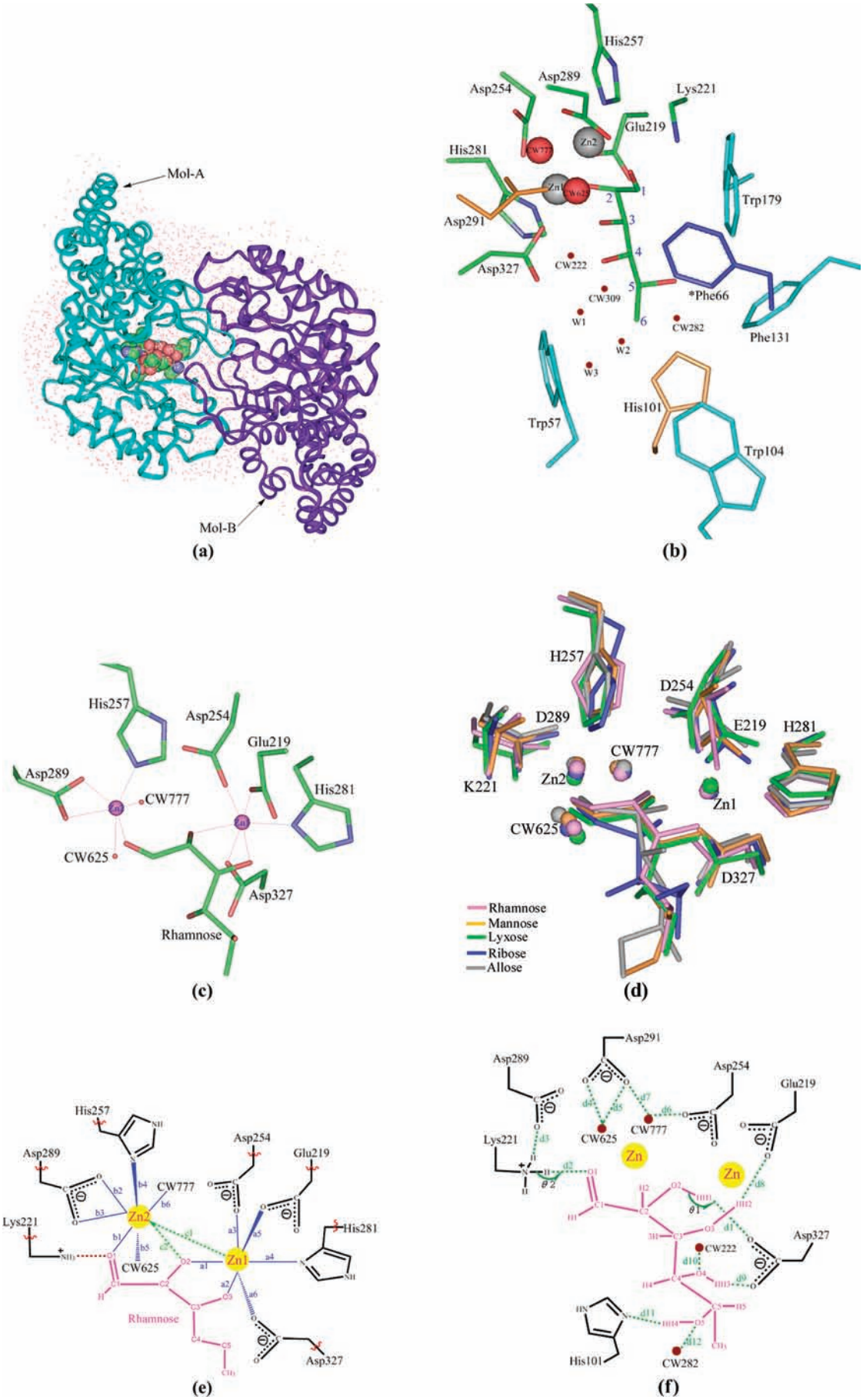

Figure 1. (a) Final equilibrium model of L-RhI after 300 ps MD simulations. (b) Key residues around the substrate-binding site. (c) Coordination shell of two zincs ions. (d) Overlap of the coordination shell of zinc ions from various complexes. (e) Selected interatomic distances around zincs. (f) Surrounding hydrogen-bond network in the active site from the equilibrated configuration.

TABLE 1: Selected Average Interatomic Distances (Å) of Various Substrate−Enzyme Complexes[a]

label[b]	rhamnose	mannose	lyxose	ribose	allose
		Interaction with Zn1			
a1 (Sub:O2)[c]	2.07 ± 0.13	2.08 ± 0.13	2.09 ± 0.13	2.07 ± 0.13	2.08 ± 0.14
a2 (Sub:O3)	2.09 ± 0.13	2.11 ± 0.14	2.11 ± 0.13	3.83 ± 1.29	4.03 ± 0.51
a3 (Asp254:OD1)	1.98 ± 0.09	1.98 ± 0.09	1.98 ± 0.09	1.97 ± 0.08	1.96 ± 0.09
a4 (His281:ND1)	2.10 ± 0.14	2.09 ± 0.13	2.08 ± 0.09	2.07 ± 0.10	2.06 ± 0.12
a5 (Glu219:OE2)	2.02 ± 0.10	2.00 ± 0.09	1.99 ± 0.10	1.99 ± 0.09	1.98 ± 0.08
a6 (Asp327:OD2)	1.99 ± 0.11	1.99 ± 0.09	1.99 ± 0.11	1.98 ± 0.10	1.98 ± 0.10
		Interaction with Zn2			
b1 (Sub:O1)	2.05 ± 0.12	2.04 ± 0.12	2.03 ± 0.1 1	2.03 ± 0.11	2.03 ± 0.11
b2 (Asp289:OD1)	2.06 ± 0.19	2.06 ± 0.12	2.08 ± 0.09	2.05 ± 0.13	2.07 ± 0.11
b3 (Asp289:OD2)	2.02 ± 0.09	2.02 ± 0.11	2.03 ± 0.11	2.02 ± 0.10	2.03 ± 0.10
b4 (His257:NE2)	2.09 ± 0.10	2.09 ± 0.12	2.08 ± 0.11	2.07 ± 0.11	2.08 ± 0.13
b5 (CW625:O)	2.03 ± 0.11	2.04 ± 0.12	2.03 ± 0.11	2.03 ± 0.10	2.03 ± 0.11
b6 (CW777:O)	2.01 ± 0.11	2.01 ± 0.10	2.01 ± 0.10	2.01 ± 0.09	2.01 ± 0.09
c1 (Zn1−Zn2)	4.84 ± 0.22	4.90 ± 0.16	5.02 ± 0.26	4.88 ± 0.18	5.06 ± 0.14
c2 (Sub:O2−Zn2)	3.02 ± 0.18	3.07 ± 0.18	3.17 ± 0.23	3.60 ± 0.39	3.69 ± 0.38

[a] The average distance over the 300 ps MD simulations in Å. [b] Refer to Figure 1e for the distance marks. [c] The distance (a1) between Zn1 and O2 from the substrate (L-rhamnose/D-allose).

TABLE 2: Selected Average Interatomic Distances between H-Bond Donor and Acceptor in Different Substrate−Enzyme Complexes[a]

label[b]	rhamnose	mannose	lyxose	ribose	allose
		Distance (Donor−Acceptor) (Å)			
d1 (Sub:HH1−Asp327:OD2)[c]	1.79 ± 0.18	2.08 ± 0.33	1.92 ± 0.29	1.78 ± 0.17	1.77 ± 0.15
d2 (Lys221:HZ2−Sub:O1)	2.04 ± 0.17	2.18 ± 0.22	2.31 ± 0.30	2.33 ± 0.33	2.32 ± 0.26
d3 (Lys221:HZ3−Asp289:OD2)	2.50 ± 0.73	2.48 ± 0.83	1.87 ± 0.23	2.30 ± 0.67	1.90 ± 0.21
d4 (CW625:HW1−Asp291:OD2)	2.25 ± 0.64	2.48 ± 0.72	2.55 ± 0.91	2.49 ± 0.86	2.69 ± 1.04
d5 (CW625:HW2−Asp291:OD1)	2.46 ± 0.81	2.47 ± 0.80	2.50 ± 0.72	2.56 ± 0.93	2.39 ± 0.71
d6 (CW777:HW3−Asp254:OD2)	2.50 ± 0.88	2.47 ± 0.82	1.81 ± 0.18	2.39 ± 0.58	2.01 ± 0.39
d7 (CW777:HW4−Asp291:OD1)	3.04 ± 1.39	2.47 ± 0.84	2.24 ± 0.57	2.70 ± 1.13	2.49 ± 0.82
d8 (Sub:HH2−Glu219:OE1)	2.48 ± 0.85	2.48 ± 0.83[e]	miss	miss	miss
d9 (Sub:HH3−Asp327:OD1)	2.30 ± 0.58	2.48 ± 0.84	1.86 ± 0.23	miss	3.09 ± 1.22[f]
d10 (CW222:H1−Sub:O4)	3.05 ± 1.16	2.48 ± 0.83	miss	miss	miss
d11 (Sub:HH4−His101:NE2)	2.46 ± 0.71	2.49 ± 0.88	3.67 ± 1.83	miss	miss
d12 (CW282:H1−Sub:O5)	3.12 ± 1.35	2.49 ± 0.84	miss	3.24 ± 1.31	miss
		Angle (deg)[d]			
θ1 (Sub−HH1−Asp327)	114 ± 18	101 ± 16	109 ± 19	95 ± 27	92 ± 34
θ2 (Sub−HZ2−Lys221)	144 ± 14	149 ± 9	144 ± 13	156 ± 11	155 ± 12

[a] The average distance over the 300 ps MD simulations in Å. [b] Refer to Figure 1f for the distance marks. [c] Sub is the abbreviation for substrate. [d] The angle of H-bond donor−H−H-bond acceptor involved in reaction. [e] The HH2−CW282 distance instead of d8. [f] The HH3−CW309 distance instead of d9.

tion. As Table 1S shows, the DFT/MM calculations and the PM3/MM MD simulations predict similar coordination shells for both zinc ions in the enzyme−substrate complexes.

For other substrates, Table 1 compiles the distances between zinc ions and their ligands at equilibrium states. The predicted structures of the active domain in Table 1 reveals that the Zn1 ion is pentacoordinated in the complexes of *P. stutzeri* L-RhI with D-ribose, and D-allose, where the interactions between Zn1 and O3 of these two substrates vanish and the separation between Zn1 and Zn2 increases slightly during MD simulations in comparison with the crystal structure. On the contrary, the coordination of the crystal water CW625 to Zn2 becomes more tightly. Interestingly, both oxygen atoms of the carboxylate group of Asp289 coordinate to Zn2, while the O2 atom of substrates departs from the coordination shell of Zn2 and interacts with Zn1 more strongly during the configurational evolution from the initial setup to the equilibrated state. In general, however, the active domains in the five investigated substrate−enzyme complexes are quite similar, and especially for the surrounding environment of metal ions, the residues involving in the metal bindings are well conserved.

There is a quite complicated hydrogen-bond network around the substrate; the selected crucial and conserved hydrogen bonds are shown in Figure 1f, and their distances are listed in Table 2. Such hydrogen bonding interactions help retain the substrate in the reaction area and mediate hydrogen transfers and thus are important for the overall enzymatic reaction. We note that the hydrogen bonds between the substrate and Lys221/Asp327 are stronger in the L-rhamnose−enzyme complex than in other complexes. Furthermore, there are abundant hydrogen-bonding interactions at the fourth, fifth, and sixth positions for the complexes of L-RhI with L-rhamnose and L-mannose, while hydrogen bonds at these positions are relatively scarce for the complexes with substrates lyxose, ribose, and allose. These hydrogen-bonding interactions predicted from PM3/MM MD simulations have been validated by the cluster-model calculations at the B3LYP level, where models with the metal-bound hydroxyl or the metal-bound water for CW777 were considered (see Figure 4S in Supporting Information for further details). The relatively strong hydrogen bonding interactions between substrates and Lys221/Asp327 have been assumed to mediate the proton transfer in the proposed mechanism for the reversible aldose−ketose isomerization (vide infra).

The conserved residues around positions 4, 5, and 6 are similar to the active site in D-XI. To gain insight into the interactions between the substrate and these residues, an energy

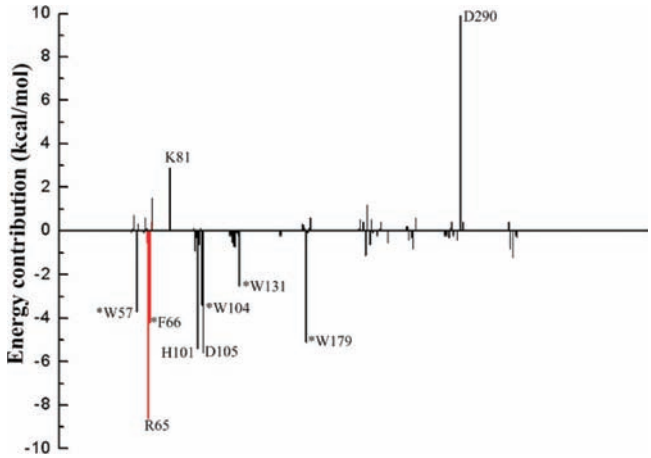

Figure 2. Electrostatic and vdW contribution of individual MM residues to stabilization and destabilization of the rhamnose−enzyme complex, where the red bar indicates the contribution of residues in chain B and the asterisk denotes that the vdW interactions are dominant.

SCHEME 2: Possible Zwitterionic Intermediate Mechanism and the Definition of Reaction Coordinates for Proton and Hydride Transfers

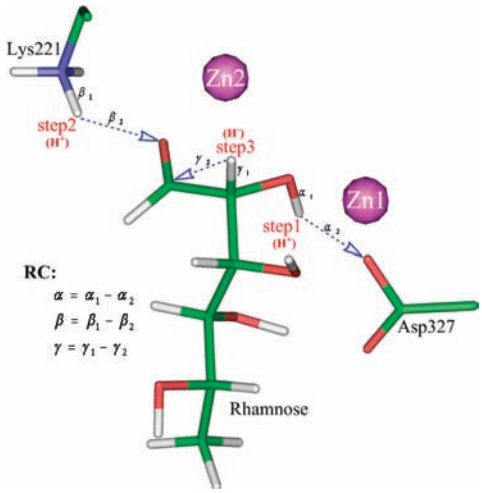

analysis including the electrostatic and van der Waals interactions between L-rhamnose and individual surrounding residues has been conducted, and the relative energy profiles from the 300 ps trajectory are depicted in Figure 2. As Figure 2 shows, there are remarkable electrostatic interactions arising from the residues His101 and Asp105 in chain A, and Arg65 in chain B, while there are dominant van der Waals interactions from the conserved residues[28] Trp57, Phe131, Phe66 in chain B, as well as Trp104 and Phe179, which may stabilize the L-rhamnose in the substrate-binding site. These results confirm that the residues at the interface from the adjoining molecule are equally important for the substrate binding, as suggested experimentally.[28]

II. Enzymatic Reaction Mechanism. Once substrates bind to *P. stutzeri* L-RhI as discussed in the above, isomerization will subsequently follow. For the enzymatic reactions of *E. coli* L-RhI[27] and D-XI,[30] a hydride shift mechanism has been proposed. After examining the hydrogen bond network in the active site, as illuminated in Figure 1f, however, we are proposing a zwitterion intermediate mechanism (Scheme 2) which comprises two proton transfers and a hydride transfer. The zwitterion intermediate as a key precursor to hydride transfer was proposed in our recently computational study on

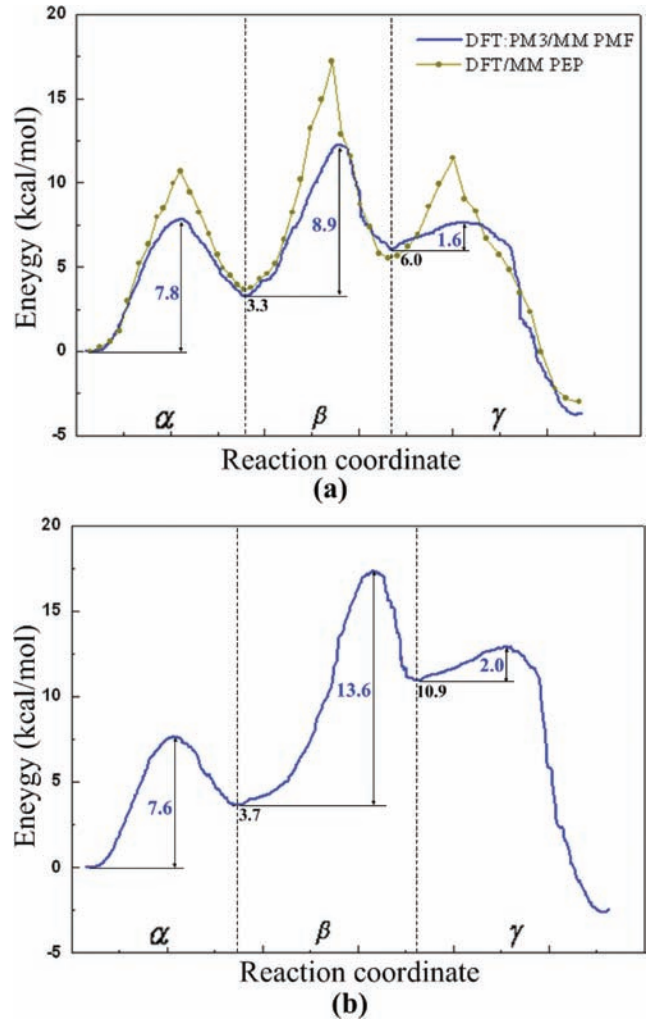

Figure 3. (a) Dual-level DFT:PM3/MM potential of mean force (PMF) and the relative QM/MM potential energy profile (PEP) for the isomerization of L-rhamnose to L-rhamnulose. (b) Dual-level DFT:PM3/MM PMF for the isomerization of D-allose to D-psicose.

the reversible aldose−ketose interconversion catalyzed by *P. furiosus* phosphoglucose isomerase.[75] As Scheme 2 shows, the isomerization starts from a first proton transfer from the substrate to the residue Asp327, followed by another proton transfer form Lys221 to the substrate to generate the zwitterion intermediate with the positive charge at C1 and the negative charge at O2 of substrate. Finally, a hydride transfer from C2 to C1 leads to the product L-rhamnulose. Presumably, the presence of a positive charge at C1 may facilitate the hydride transfer process.

To validate this zwitterion intermediate mechanism involving three steps, we carried out PM3/MM MD simulations and explored the thermodynamic and dynamic properties of the reversible isomerization of L-rhamnose to L-rhamnulose along the reaction coordinates, which are generally defined as the differences between the distances of breaking bonds and forming bonds (see Scheme 2). Parts a and b of Figure 3 present the dual-level PMFs for the reversible isomerizations of L-rhamnose to L-rhamnulose and D-allose to D-psicose, respectively. Figure 4 displays the time evolution of selected structural parameters along the reaction pathways.

As shown in Figure 3, both reactions have similar PMF profiles and the hydride transfer in the third step is quite facile. The rate-determining step is the second proton transfer from Lys221 to O1 of the substrate, and the free energy barrier in this step is 8.9 kcal/mol for L-rhamnose (Figure 3a), about 4.7

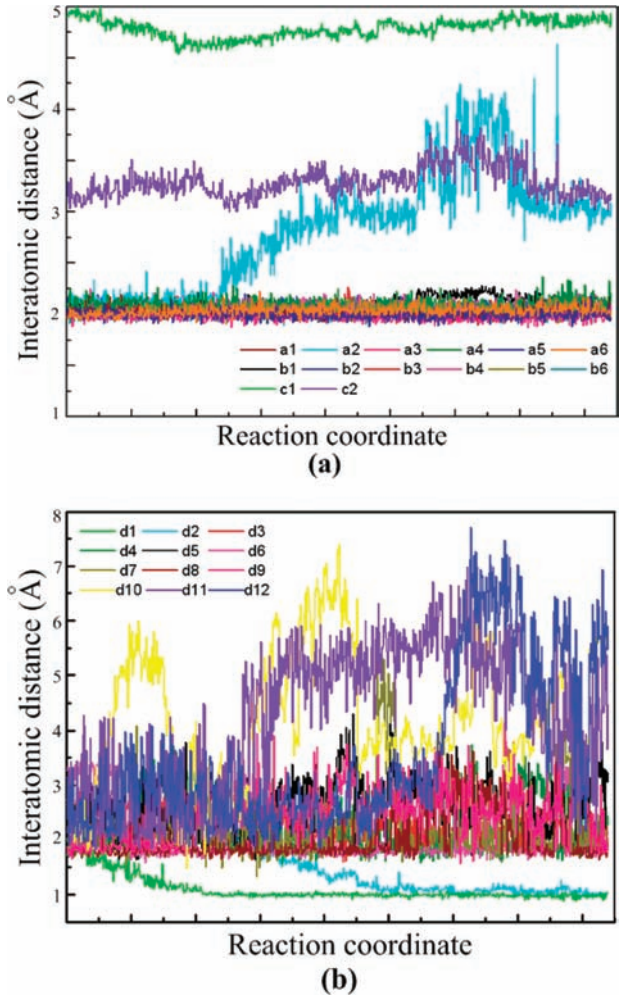

Figure 4. (a) Evolution of the coordination shell of zinc ions along the reaction process. (b) Evolution of hydrogen-bond distances along the reaction process.

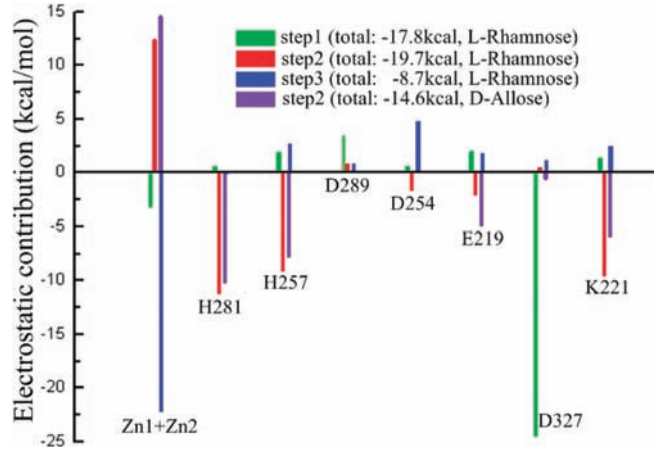

Figure 5. Electrostatic contribution of individual residues in the QM region to stabilization and destabilization of the rhamnose−enzyme complex at the different steps.

kcal/mol lower than D-allose (Figure 3b). Within the transition state theory, an approximately estimated overall activation energy difference between L-rhamnose and D-allose is about 4.2 kcal/mol based on the experimental kinetic data.[26] In consideration of comparable barriers in the first and third steps for both substrates, the predicted free energy barrier difference of 4.7 kcal/mol in the second step can be regarded as a good agreement with the experimental evidence.

Along the reaction pathway, we note that the zwitterion configuration is of a slightly higher energy than the initial state by 6 kcal/mol for L-rhamnose and 10.9 kcal/mol for D-allose, and a similar zwitterionic state of substrate was involved in the enzymatic reaction of the phosphoglucose isomerase[75] and the cysteine proteases.[76] As Figures 1 and 4 show, the coordination shells of the metal ions are nearly conserved in the reaction processes, except that the O3−Zn1 bonding gradually vanishes. At the same time, the hydrogen bond network is remarkably adjusted as the reaction proceeds, as many hydrogen bonds at the fourth, fifth, and sixth positions weaken or even disappear. Such reshufflings actually facilitate the release of the product in the end.

The potential energy profile (PEP) along the reaction coordinates has also been estimated by using the energy scan at the B3LYP/CHARMM level. Compared with the dual-level DFT: PM3/MM MD simulations, the QM(B3LYP)/MM energy scan results in remarkably increased energy barriers for all three steps, as Figure 3a shows, though interestingly the latter increases the three barriers in a similar scale. It is worthwhile to note that the energy scan computes the energies at separated points and thus the important entropy contribution that plays a stabilizing role is not considered. For comparison, the dual-level DFT: PM3/MM MD simulations take the dynamical movement of the whole system into account and thus is more reliable than the energy scans.

To probe the catalytic roles of the residues included in the QM region, we evaluated their classical electrostatic contributions to the relative energetics of different key states (including the reactant, intermediate, transition, and product states) by ensemble averaging and summarizing. As shown in Figure 5, these residues totally contribute about 18 kcal/mol to the stabilization of the transition state in the first step in the isomerization of L-rhamnose to L-rhamnulose, 20 kcal/mol in the rate-determining step, and 9 kcal/mol in the third step. The most remarkable contribution in the first step is from Asp327, which acts as the proton acceptor in the initial proton transfer. In the second step, the residues H281, H257, K221, and both zinc ions have comparable electrostatic energy contributions, where the metal ions exhibit destabilizing interactions. Apparently, the hydride shift step is basically mediated by the zinc ions, especially by the "catalytic" metal Zn2.

Significantly yet interestingly, we found that the PM3/MM PMF barrier is higher than the dual-level PMF barrier by as much as 18 kcal/mol, as demonstrated in Figure 3S (see Supporting Information), and we speculate that such notable discrepancy arises from the poor description of electrostatic energy in the transition state at the PM3 level. Figure 5 reveals that the energy difference in the second step from the electrostatic interactions is about 5 kcal/mol for the isomerizations of L-rhamnose and D-allose, which is comparable to the corresponding free energy barrier difference in the same step as shown in Figure 3. As Figure 3S shows, the maximum deviation of PM3/MM PMF appears at the transition state in comparison with the dual level approach, and the relative single energy from the partial optimization in the gas phase shows similar trends.

The remarkable movement of the metal center and the hydride transfer were proposed for reactions in both D-XI isomerase[77,78] and phosphotriesterase.[59] On the contrary, the metal ions of *P. stutzeri* L-RhI move negligibly in our MD simulations, and the bimetal distance between Zn1 and Zn2 is only slightly fluctuated within ±0.25 Å in the proton transfer and hydride transfer steps.

The hexacoordinated structural environment of zinc ions in *P. stutzeri* L-RhI makes the metal dynamic motion become difficult in reactions.

III. Substrate Specificity. The X-ray crystal structure of *E. coli* L-RhI[28] revealed that there is an unique hydrophobic pocket at the positions 4, 5, and 6 of substrate, which is responsible for the strict substrate recognition. As a consequence, only L-rhamnose is the suitable substrate which is able to dock into the reactive site of *E. coli* L-RhI. In contrast, the crystal structure of *P. stutzeri* L-RhI showed that Phe66 from another chain B extends into the active site in chain A and no hydrophobic pocket like in *E. coli* L-RhI was observed. Our QM/MM MD simulations show that there is a large vacancy around the fourth, fifth, and sixth positions of substrates for *P. stutzeri* L-RhI and a few water molecules even can enter into the active domain of the complexes of the enzyme with substrates L-rhamnose, L-mannose, L-lyxose, D-ribose, and D-allose, leading to a typical hydrophilic microenvironment. Such structural features of the substrate-binding site and the van der Waals and electrostatic interactions between substrates and the conserved residues lead to the broad substrate recognition, which concerns only the configurations of the first three positions of substrates as observed experimentally. Furthermore, we note that the coordination shells of the metal ions are pretty much conserved regardless of the substrate substitution in the MD simulations.

In the present zwitterion intermediate mechanism, the isomerization was driven by proton transfers between the surrounding residues and the moieties of C2−O2 and O1−C1 of the substrate, and thus the configurations of O1−C1 and O2−C2 positions are very crucial for the enzyme activity. Similar structural features and hydrogen bond interactions in the C1 and C2 region (see Figure 1c, Table 1 and Table 2) of the substrate-binding site for substrates L-rhamnose, L-mannose, L-lyxose, D-ribose, and D-allose make them serve as suitable substrates for *P. stutzeri* L-RhI. However, the differences of hydrogen bond network at positions 4, 5, and 6 and the coordination interaction between O3 and Zn1 for these substrates may slightly influence their relative reactivity in *P. stutzeri* L-RhI. As Tables 1 and 2 show, the presence of O3−Zn1 bond and hydrogen bond interactions at the fourth, fifth, and sixth positions may retain the substrate in the reactive region nicely, leading to relatively higher activity for substrates L-rhamnose, L-mannose, and L-lyxose as compared with D-ribose and D-allose. This difference in relative activity was observed experimentally[26] and interpreted by the dual-level QM/MM MD simulations.

Conclusion

Combined QM/MM MD simulations have been conducted to explore the aldose-ketose isomerization catalyzed by *P. stutzer* L-RhI, and a zwitterion intermediate-based mechanism involving proton and hydride transfers was examined. In the reversible isomerization, the residues Asp327 and Lys221, serving as the general acid and base, mediate the proton transfers between the substrate and surrounding residues, leading a zwitterion intermediate. Following a facile hydride transfer, the zwitterion evolves into the product. The barriers derived from the dual-level MD simulations at the rate-determining step are 8.9 and 13.6 kcal/mol for L-rhamnose and D-allose, respectively, and this predicted disparity in relative activity of *P. stutzer* L-RhI toward both substrates is in agreement with experimental observations.[26] The roles of the key residues and the zinc ions in the enzymatic reaction and the substrate specificity have been discussed on the basis of the electrostatic interaction analysis and the dynamic structural features from the MD simulations. Calculations and simulations show that the residues at the interface from the neighboring molecule and the hydrogen bonding interactions around the substrate are important for the enzymatic process. Albeit a broad substrate specificity, *P. stutzer* L-RhI exhibits a keen difference in its activity toward various substrates. Our analyses suggest that the slight differences in the coordination shell of Zn1 and in the hydrogen bond network at the fourth, fifth, and sixth positions are responsible for the relative activities of substrates L-rhamnose, L-mannose, L-lyxose, D-ribose, and D-allose.

Acknowledgment. This work was supported by the National Science Foundation of China (20673087, 20733002, 20873105) and the Ministry of Science and Technology (2004CB719902).

Supporting Information Available: Superimposition of the XRD structure (pdb code: 2I56) and the equilibrium configuration after 300 ps PM3/MM MD simulations for *P. stutzeri* L-RHI, comparison of potential of mean force from various umbrella sampling times for each windows at the PM3/MM level for the first step catalyzed by L-RHI, the QM energy profiles calibrated by high-level DFT calculations for the dual-level MD simulations, comparison of interatomic distances by theory and experiment, and selected B3LYP-optimized structures of different initial cluster models. This material is available free of charge via the Internet at http://pubs.acs.org.

References and Notes

(1) Muniruzzaman, S.; Tokunaka, H.; Izumori, K. *J. Ferment. Bioeng.* **1994**, *78*, 145.
(2) Itoh, H.; Sato, T.; Takuchi, T.; Khan, A. R.; Izumori, K. *J. Ferment. Bioeng.* **1995**, *79*, 184.
(3) Izumori, K. *Naturwissenschaften* **2002**, *89*, 120.
(4) Kim, P.; Yoon, S. H.; Roh, H. J.; Choi, J. H. *Biotechnol. Prog.* **2001**, *17*, 208.
(5) Leang, K.; Sultana, I.; Takada, G.; Izumori, K. *J. Biosci. Bioeng.* **2003**, *95*, 310.
(6) Berrisford, J. M.; Hounslow, A. M.; Akerboom, J.; Hagen, W. R.; Brouns, S. J. J.; van der Oost, J.; Murray, I. A.; Blackburn, G. M.; Waltho, J. P.; Rice, D. W.; Baker, P. J. *J. Mol. Biol.* **2006**, *358*, 1353.
(7) Hansen, T.; Schlichting, B.; Felgendreher, M.; Schönheit, P. *J. Bacteriol.* **2005**, *187*, 1621.
(8) Swan, M. K.; Hansen, T.; Schonheit, P.; Davies, C. *J. Biol. Chem.* **2004**, *279*, 39838.
(9) Hansen, T.; Wendorff, D.; Schonheit, P. *J. Biol. Chem.* **2004**, *279*, 2262.
(10) Wong, H. C.; Ting, Y.; Lin, H. C.; Reichert, F.; Myambo, K.; Watt, K. W. K.; Toy, P. L.; Drummond, R. *J. Bacteriol.* **1991**, *173*, 6849.
(11) Izumori, K.; Yamanaka, K. *Agric. Biol. Chem.* **1974**, *38*, 267.
(12) Kim, B. C.; Lee, Y. H.; Lee, H. S.; Lee, D. W.; Choe, E. A.; Pyun, Y. R. *FEMS Microbiol. Lett.* **2000**, *212*, 121.
(13) Moralejo, P. *J. Bacteriol.* **1993**, *175*, 5585.
(14) Lavie, A.; Allen, K. N.; Petsko, G. A.; Ringe, D. *Biochemistry* **1994**, *33*, 5469.
(15) Hess, J. M.; Tchernajenko, V.; Vieille, C.; Zeikus, J. G.; Kelly, R. M. *Appl. Environ. Microbiol.* **1998**, *64*, 2357.
(16) Wilson, D. M.; Ajl, S. *J. Bacteriol.* **1957**, *73*, 410.
(17) Englesberg, E.; Baron, L. S. *J. Bacteriol.* **1959**, *78*, 675.
(18) Domagk, G. F.; Zech, R. *Biochem. Z.* **1963**, *339*, 145.
(19) Bhuiyan, S. H. *J. Ferment. Bioeng.* **1997**, *84*, 319.
(20) Bhuiyan, S. H. *J. Ferment. Bioeng.* **1997**, *84*, 558.
(21) Bhuiyan, S. H. *J. Ferment. Bioeng.* **1998**, *85*, 539.
(22) Bhuiyan, S. H. *J. Biosci. Bioeng.* **1999**, *88*, 567.
(23) Menavuvu, B. T.; Poonperm, W.; Leang, K.; Noguchi, N.; Okada, H.; Morimoto, K.; Granstrom, T. B.; Takada, G.; Izumori, K. *J. Biosci. Bioeng.* **2006**, *101*, 340.
(24) Menavuvu, B. T.; Poonperm, W.; Takeda, K.; Morimoto, K.; Grand, E.; Takada, G.; Izumori, K. *J. Biosci. Bioeng.* **2006**, *102*, 436.
(25) Leang, K.; Takada, G.; Ishimura, A.; Okita, M.; Izumori, K. *Appl. Environ. Microbiol.* **2004**, *70*, 3298.
(26) Leang, K.; Takada, G.; Fukai, Y.; Morimoto, Y.; Granstrom, T. B.; Izumori, K. *Biochim. Biophysi. Acta-Gen. Subj.* **2004**, *1674*, 68.
(27) Korndorfer, I. P.; Fessner, W. D.; Matthews, B. W. *J. Mol. Biol.* **2000**, *300*, 917.

(28) Yoshida, H.; Yamada, M.; Ohyama, Y.; Takada, G.; Izumori, K.; Kamitori, S. *J. Mol. Biol.* **2007**, *365*, 1505.
(29) Yoshida, H.; Yamaji, M.; Yamada, M.; Takada, G.; Izumori, K.; Ishii, T.; Kamitori, S. *FEBS J.* **2007**, *274*, 271.
(30) Whitlow, M.; Howard, A. J.; Fingel, B. C.; Poulos, T. L.; Winborne, E.; Gilliland, G. L. *Proteins: Struct., Funct., Genet.* **1991**, *9*, 153.
(31) Field, M. J.; Bash, P. A.; Karplus, M. *J. Comput. Chem.* **1990**, *11*, 700.
(32) Monard, G.; Merz, K. M. *Acc. Chem. Res.* **1999**, *32*, 904.
(33) Zhang, Y. K.; Liu, H.; Yang, W. T. *J. Chem. Phys.* **2000**, *112*, 3483.
(34) Cui, Q.; Guo, H.; Karplus, M. J. *J. Chem. Phys.* **2002**, *117*, 5617.
(35) Warshel, A. *Annu. Rev. Biophys. Biomol. Struct.* **2003**, *32*, 425.
(36) Karplus, M.; Kuriyan, J. *Proc. Natl. Acad. Sci. U.S.A.* **2005**, *102*, 6679.
(37) Bruice, T. C. *Chem. Rev.* **2006**, *106*, 3119.
(38) Gao, J.; Ma, S.; Major, D. T.; Nam, K.; Pu, J.; Truhlar, D. G. *Chem. Rev.* **2006**, *106*, 3188.
(39) Hu, P.; Zhang, Y. *J. Am. Chem. Soc.* **2006**, *128*, 1272.
(40) Lin, H.; Truhlar, D. G. *Theor. Chem. Acc.* **2007**, *117*, 185.
(41) Senn, H. M.; Thiel, W. QM/MM methods for biological systems. In *Atomistic Approaches in Modern Biology: from Quantum Chemistry to Molecular Simulations*; Springer-Verlag: Berlin, 2007; Vol. 268, p 173.
(42) Hong, G. Y.; Strajbl, M.; Wesolowski, T. A.; Warshel, A. *J. Comput. Chem.* **2000**, *21*, 1554.
(43) Crespo, A.; Scherlis, D. A.; Martí, M. A.; Ordejón, P.; Roitberg, A. E.; Estrin, D. A. *J. Phys. Chem. B* **2003**, *107*, 13728.
(44) Hu, P.; Wang, S.; Zhang, Y. *J. Am. Chem. Soc.* **2008**, *130*, 3806.
(45) Dewar, M. J. S.; Zoebisch, E. G.; Healy, E. F.; Stewart, J. J. P. *J. Am. Chem. Soc.* **1985**, *107*, 3902.
(46) Stewart, J. J. P. *J. Comput. Chem.* **1989**, *10*, 209.
(47) Elstner, M. *Theor. Chem. Acc.* **2006**, *116*, 316.
(48) Rossi, I.; Truhlar, D. G. *Chem. Phys. Lett.* **1995**, *234*, 64.
(49) Winget, P.; Horn, A. H. C.; Selcuki, C.; Martin, B.; Clark, T. *J. Mol. Model.* **2003**, *9*, 408.
(50) Thiel, W.; Voityuk, A. A. *Theor. Chim. Acta* **1992**, *81*, 391.
(51) Lopez, X.; York, D. M. *Theor. Chem. Acc.* **2003**, *109*, 149.
(52) Thuy, T. T. T.; Liou, K.; Oh, T. J.; Kim, D. H.; Nam, D. H.; Yoo, J. C.; Sohng, J. K. *Glycobiology* **2007**, *17*, 119.
(53) Byun, K.; Mo, Y.; Gao, J. *J. Am. Chem. Soc.* **2001**, *123*, 3974.
(54) Proust-De Martin, F.; Dumas, R.; Field, M. J. *J. Am. Chem. Soc.* **2000**, *122*, 7688.
(55) Brothers, E. N.; Suarez, D.; Deerfield, D. W., II; Merz, K. M., Jr. *J. Comput. Chem.* **2004**, *25*, 1677.
(56) Bräuer, M.; Kunert, M.; Dinjus, E.; Kluszmann, M.; Doring, M.; Gorls, H.; Anders, E. *J. Mol. Struct. (THEOCHEM)* **2000**, *505*, 289.
(57) Svensson, M.; Humbel, S.; Froese, R. D.; Morokuma, K. *J. Phys. Chem. A* **1997**, *101*, 227.
(58) Martí, S.; Moliner, V.; Tunon, I. *J. Chem. Theory Comput.* **2005**, *1*, 1008.
(59) Kin-Yiu, W.; Gao, J. *Biochemistry* **2007**, *46*, 13352.
(60) Frisch, M. J.; Trucks, G. W.; Schlegel, H. B.; Scuseria, G. E.; Robb, M. A.; Cheeseman, J. R.; Montgomery, J. A., Jr.; Vreven, T.; Kudin, K. N.; Burant, J. C.; Millam, J. M.; Iyengar, S. S.; Tomasi, J.; Barone, V.; Mennucci, B.; Cossi, M.; Scalmani, G.; Rega, N.; Petersson, G. A.; Nakatsuji, H.; Hada, M.; Ehara, M.; Toyota, K.; Fukuda, R.; Hasegawa, J.; Ishida, M.; Nakajima, T.; Honda, Y.; Kitao, O.; Nakai, H.; Klene, M.; Li, X.; Knox, J. E.; Hratchian, H. P.; Cross, J. B.; Bakken, V.; Adamo, C.; Jaramillo, J.; Gomperts, R.; Stratmann, R. E.; Yazyev, O.; Austin, A. J.; Cammi, R.; Pomelli, C.; Ochterski, J. W.; Ayala, P. Y.; Morokuma, K.; Voth, G. A.; Salvador, P.; Dannenberg, J. J.; Zakrzewski, V. G.; Dapprich, S.; Daniels, A. D.; Strain, M. C.; Farkas, O.; Malick, D. K.; Rabuck, A. D.; Raghavachari, K.; Foresman, J. B.; Ortiz, J. V.; Cui, Q.; Baboul, A. G.; Clifford, S.; Cioslowski, J.; Stefanov, B. B.; Liu, G.; Liashenko, A.; Piskorz, P.; Komaromi, I.; Martin, R. L.; Fox, D. J.; Keith, T.; Al-Laham, M. A.; Peng, C. Y.; Nanayakkara, A.; Challacombe, M.; Gill, P. M. W.; Johnson, B.; Chen, W.; Wong, M. W.; Gonzalez, C.; Pople, J. A. *Gaussian 03*; Gaussian, Inc.: Wallingford CT, 2004.
(61) Brooks, B. R.; Bruccoleri, R. E.; Olafson, B. D.; States, D. J.; Swaminathan, S.; Karplus, M. *J. Comput. Chem.* **1983**, *4*, 187.
(62) Gao, J. L.; Amara, P.; Alhambra, C.; Field, M. J. *J. Phys. Chem. A* **1998**, *102*, 4714.
(63) MacKerell, A. D.; Bashford, D.; Bellott, M.; et al. *J. Phys. Chem. B* **1998**, *102*, 3586.
(64) MacKerell, A. D.; Feig, M.; Brooks, C. L. *J. Comput. Chem.* **2004**, *25*, 1400.
(65) van Gunsteren, W. F.; Berendsen, H. J. C. *Mol. Phys.* **1977**, *34*, 1311.
(66) Berkowitz, M.; McCammon, J. A. *Chem. Phys. Lett.* **1982**, *90*, 215.
(67) Jorgensen, W. L.; Chandrasckhar, J.; Madura, J. D.; Impey, R. W.; Klein, M. L. *J. Chem. Phys.* **1983**, *79*, 926.
(68) Bakowies, D.; Thiel, W. *J. Phys. Chem.* **1996**, *100*, 10580.
(69) de Vries, R. P.; Jansen, J.; Aguilar, G.; Parenicova, L.; Joosten, V.; Wulfert, F.; Benen, J. A. E.; Visser, J. *FEBS Lett.* **2002**, *530*, 41.
(70) Sherwood, P.; de Vries, A. H.; Collins, S. J.; Greatbanks, S. P.; Burton, N. A.; Vincent, M. A.; Hillier, I. H. *Faraday Discuss.* **1997**, *106*, 79.
(71) Sherwood, P.; de Vries, A. H.; Guest, M. F.; Schreckenbach, G.; Catlow, C. R. A.; French, S. A.; Sokol, A. A.; Bromley, S. T.; Thiel, W.; Turner, A. J.; Billeter, S.; Terstegen, F.; Thiel, S.; Kendrick, J.; Rogers, S. C.; Casci, J.; Watson, M.; King, F.; Karlsen, E.; Sjovoll, M.; Fahmi, A.; Schafer, A.; Lennartz, C. *J. Mol. Struct. (THEOCHEM)* **2003**, *632*, 1.
(72) Ahlrichs, R.; Bar, M.; Haser, M.; Horn, H.; Kolmel, C. *Chem. Phys. Lett.* **1989**, *162*, 165.
(73) Smith, W.; Forester, T. R. *J. Mol. Graph.* **1996**, *14*, 136.
(74) Billeter, S. R.; Turner, A. J.; Thiel, W. *Phys. Chem. Chem. Phys.* **2000**, *2*, 2177.
(75) Wu, R.; Xie, H.; Cao, Z.; Mo, Y. *J. Am. Chem. Soc.* **2008**, *130*, 7022.
(76) Mladenovic, M.; Fink, R. F.; Thiel, W.; Schirmeister, T.; Engels, B. *J. Am. Chem. Soc.* **2008**, *130*, 8696.
(77) Allen, K. N.; Lavie, A.; Petsko, G. A.; Ringe, D. *Biochemistry* **1995**, *34*, 3742.
(78) Garcia-Viloca, M.; Alhambra, C.; Truhlar, D. G.; Gao, J. *J. Am. Chem. Soc.* **2002**, *124*, 7268.

JP901093G